SANDIA REPORT

SAND2008-03690369
Unlimited Release
Printed January 2008

MEMS Lubrication by In-Situ Tribochemical Reactions From the Vapor Phase

Michael T. Dugger, David B. Asay and Seong H. Kim

Prepared by
Sandia National Laboratories
Albuquerque, New Mexico 87185 and Livermore, California 94550

Sandia is a multiprogram laboratory operated by Sandia Corporation,
a Lockheed Martin Company, for the United States Department of Energy's
National Nuclear Security Administration under Contract DE-AC04-94AL85000.

Issued by Sandia National Laboratories, operated for the United States Department of Energy by Sandia Corporation.

Available to DOE and DOE contractors from
U.S. Department of Energy
Office of Scientific and Technical Information
P.O. Box 62
Oak Ridge, TN 37831

Telephone: (865)576-8401
Facsimile: (865)576-5728
E-Mail: reports@adonis.osti.gov
Online ordering: http://www.osti.gov/bridge

Available to the public from
U.S. Department of Commerce
National Technical Information Service
5285 Port Royal Rd
Springfield, VA 22161

Telephone: (800)553-6847
Facsimile: (703)605-6900
E-Mail: orders@ntis.fedworld.gov
Online order: http://www.ntis.gov/help/ordermethods.asp?loc=7-4-0#online

SAND2008-xxxx
Unlimited Release
Printed January 2008

MEMS Lubrication by In-Situ Tribochemical Reactions from the Vapor Phase

Michael T. Dugger[1], David B. Asay[2] and Seong H. Kim[2]

[1]Materials Science and Engineering Center, Sandia National Laboratories
Albuquerque, New Mexico

[2]Department of Chemical Engineering, the Pennsylvania State University
University Park, Pennsylvania

Abstract

Vapor Phase Lubrication (VPL) of silicon surfaces with pentanol has been demonstrated. Two potential show stoppers with respect to application of this approach to real MEMS devices have been investigated. Water vapor was found to reduce the effectiveness of VPL with alcohol for a given alcohol concentration, but the basic reaction mechanism observed in water-free environments is still active, and devices operated much longer in mixed alcohol and water vapor environments than with chemisorbed monolayer lubricants alone. Complex MEMS gear trains were successfully lubricated with alcohol vapors, resulting in a factor of 10^4 improvement in operating life *without failure*. Complex devices could be made to fail if operated at much higher frequencies than previously used, and there is some evidence that the observed failure is due to accumulation of reaction products at deeply buried interfaces. However, if hypothetical reaction mechanisms involving heated surfaces are valid, then the failures observed at high frequency may not be relevant to operation at normal frequencies. Therefore, this work demonstrates that VPL is a viable approach for complex MEMS devices in conventional packages. Further study of the VPL reaction mechanisms are recommended so that the vapor composition may be optimized for low friction and for different substrate materials with potential application to conventionally fabricated, metal alloy parts in weapons systems. Reaction kinetics should be studied to define effective lubrication regimes as a function of the partial pressure of the vapor phase constituent, interfacial shear rate, substrate composition, and temperature.

Acknowledgments

The authors are indebted to Tony Ohlhausen of Sandia's surface analysis laboratory for assistance with the ToF-SIMS spectral data, and to Michael Rye of Sandia's microscopy laboratory for MEMS device disassembly and microscopy. Pre-publication technical review by Somuri Prasad was appreciated. Funding from the Nanoscience to Microsystems LDRD investment area is gratefully acknowledged.

Contents

List of Figures

List of Tables

Page

Nomenclature

AFM	Atomic Force Microscope
ATR-FTIR	Attenuated Total Internal Reflectance Fourier Transform Infrared Spectroscopy
DIP	(Ceramic) Dual in Line Package
DMS	Discriminating Micro Switch
FIB	Focused Ion Beam
FOTAS	perfluoro-octyltris(dimethylamino)silane, $C_8F_{13}H_4Si(CH_3CH_3N)_3$
MEMS	MicroElectroMechanical System
SEM	Secondary Electron Microscopy
SNL	Sandia National Laboratories
ToF-SIMS	Time-of-Flight Secondary Ion Mass Spectrometry
VPL	Vapor Phase Lubrication
VSAM	Vapor-deposited Self-Assembled Monolayer
XPS	X-ray Photoelectron Spectroscopy

1. Introduction

1.1 Scope of This Report

This report describes the results of a late-start Laboratory Directed Research and Development (LDRD) project (proposal 07-1607, Oracle project number 113217) to investigate two potential show-stoppers associated with a new lubrication scheme for microsystems developed in partnership with the University of Pennsylvania. The new lubrication scheme is known as "vapor phase lubrication" or VPL. The work described here was conducted between March and September 2007, with a total budget of $99k.

1.2 The Vapor Phase Lubrication Innovation

The application of VPL to microsystems is described in detail in Sandia Technical Advance #10564. Briefly, organic molecules in the vapor phase adsorb on silicon surfaces and impart remarkable operational reliability to MicroElectroMechanical Systems (MEMS) that rely on contacting and sliding surfaces. This is accomplished by elimination of measurable wear, and maintaining acceptably low friction coefficient through dynamic replenishment of a surface reaction product.

The concept of vapor phase lubrication is not a new one in tribology. This approach was first conceived for lubrication of metallic super alloy contacts at high temperature [1.1], where traditional liquid lubricants decompose and solid lubricants exhibit limited life due to their one-time application on sliding surfaces. The essential concept was to provide a source of lubricating material that could be continuously replenished as the lubricating layer was removed by wear. These early efforts relied upon delivery of carbonaceous cases such as methane or acetylene to heated nickel-based super alloy surfaces in the absence of oxygen. At the hot surface the gases would decompose rather than burn, and deposit a layer of amorphous carbon. The amorphous carbon film provided high temperature solid lubrication, and deposition continued as long as an active metal surface and the carbon-rich gas were present.

The application of the VPL concept to MEMS did not evolve directly from earlier work on macroscale heated contacts. The connection was not initially obvious, perhaps due to the perceived need for surfaces heated to high temperature to facilitate gas decomposition, which would introduce a significant energy penalty to the usual low power requirements of MEMS operation. The successful demonstration of VPL of silicon grew out of interactions between staff at Sandia National Laboratories and the Pennsylvania State University begun in 2004, both of whom were working to mitigate friction and adhesion between MEMS surfaces.

One of the authors' (MTD) research efforts concentrated on metrology and fundamental understanding of friction in MEMS interfaces. Research programs as of 2005 had dealt with aging of chemisorbed monolayers, one of the conventional approaches to facilitate release of MEMS devices to avoid capillary adhesion caused by water adsorption [1.2-1.3]. Significant research has been performed at Sandia and other institutions to understand the role of chain length, end group chemistry, and processing on the adhesion

and friction of "self-assembled monolayer," or SAM films. The "self-assembled" moniker is derived from the concept that these molecules have an active group on one end and can react with specific chemical sites on the surface. Siloxane, or Si-O, attachment chemistry is common in SAM films because the silicon oxygen bond is one of the strongest available for attaching hydrocarbon or fluorocarbon films to silicon surfaces. However, there is yet no definitive measurement of the actual density of siloxane bonds at a SAM/substrate interface, and the films may contain significant hydrogen bonding as well. In addition, stearic constraints and disorder at grain boundaries are expected to result in significant defect density in the as-deposited films on polycrystalline silicon [1.4]. As a result, SAM films are known to be susceptible to removal by hydrolysis if any water vapor is present [1.5]. More importantly, even molecules that are very reactive with silicon such as tridecafluorotris (dimethylamino)silane, $CF_3(CF_2)_5$-$(CH_2)_2Si(N(CH_3)_2)_3$ or "FOTAS," deposited from the vapor phase (VSAM) to improve reproducibility, are damaged very easily under very modest contact forces at MEMS interfaces [1.6].

Limited additional research in one of the authors' laboratories (MTD) had been funded over the past decade to explore alternative surface treatments and alternate materials for MEMS. One of the surface treatment approaches involves atomic layer deposition, or ALD, of tungsten disulfide thin films [1.7]. The ALD process creates highly conformal coatings with atomic control of thickness, but is not typically selective so that semiconductors such as WS_2 create electrical shorts between traces on the wafer. Work at other institutions has explored deposition of TiO_2 thin films by ALD [1.8], but these can interfere with electrical signals and still suffer from capillary adhesion due to adsorbed water. Selective tungsten is a common process for producing electrical interconnect vias and is selective to silicon, so that electrical isolation can be maintained. However, the process produces surface flaws that reduce mechanical strength in polycrystalline structures from ~2.5 to ~1.0 GPa [1.9]. Chemical vapor deposited SiC thin films [1.10] have proven to be wear resistant, but involve high temperature processing and can also suffer from adhesion effects, although the adhesion energy appears to be lower than that of the polycrystalline silicon surface due in part to increased roughness. Further, any coatings applied after release have the potential to fuse surfaces together for structures that are in mechanical contact during the coating deposition process.

While work on hard surface coatings was proceeding, work in another of the authors' laboratories (SHK) involved reducing adhesion by adsorbing alcohol on silicon surfaces [1.11]. Adhesion modeling and experiments with AFM tips indicated that adsorption of alcohols could significantly reduce adhesion because of their low surface energy, limited adsorbed film thickness, and high molar volume [1.12]. Wear was also found to be absent when a silicon tip was rubbed on a silicon wafer in argon containing propanol vapor, compared to a measurable wear groove formed under identical contact conditions when sliding in air at 75% relative humidity. The mechanism for this wear reduction was not understood, however. In the summer of 2006, experiments at Sandia demonstrated that this wear reduction also occurred when sliding a 3.2 mm diameter silica ball against a silicon wafer surface in pentanol vapor [1.13]. ToF-SIMS surface analysis of wear tracks showed that at the highest pressure location within the wear tracks (the center), a

high molecular weight reaction product formed. This reaction product was found to build up on the track during the initial stages of sliding and prevent subsequent wear of the silicon surfaces. Experiments using MEMS sidewall friction diagnostic structures indicated that this process also occurred in MEMS device contacts. Friction devices coated with chemisorbed FOTAS films alone operated for less than 10^4 cycles in dry N_2, while devices with the same coating operated in N_2 with pentanol vapor for up to 10^8 cycles without failure. Devices were operated in test environments from 15 to 95% of the saturation pressure of pentanol (2.3 mbar at 21ºC), and all were stopped intentionally for analysis at more than 10^6 cycles rather than stopping due to failure [1.14].

1.3 Potential VPL Show Stoppers for MEMS

With the apparent dramatic success of VPL in improving the operating life of silicon micromachined diagnostic devices, two potential issues with application to real MEMS devices were envisioned. One potential show stopper involves the presence of water vapor in the operating environment, which may compete with the organic molecules for adsorption on the surface and therefore interfere with reaction product formation. The second potential show stopper concerned the build-up of reaction product in narrow gaps. If the high molecular weight reaction product were formed at a buried interface such that it could not be displaced outside the contact, the reaction product may eventually accumulate to the point where it could impede device operation. The main purpose of this work, therefore, was to establish whether vapor phase lubrication of silicon with pentanol would be successful in the presence of some water vapor consistent with packaging levels, and to demonstrate VPL of a complex MEMS device with buried sliding interfaces.

Chapter 1 References

1.1 J.L. Lauer, T.B. Blanchet, B.L. Vlcek and B.L. Sargent, "Lubrication of Si_3N_4 and Steel Rolling and Sliding Contacts by Deposits of Pyrolyzed Carbonaceous Gases" *Surface and Coatings Technology* **62** (1993) p.399-405.

1.2 M.T. Dugger, R.J. Hohlfelder and D.E. Peebles, "Degradation of Monolayer Lubricants for MEMS," in *Proc. SPIE - The International Society for Optical Engineering,* **4980** (2003) R. Ramesham and D.M. Tanner, Eds., p.138-150.

1.3 M.T. Dugger, D.M. Tanner, J.A. Walraven, J.V. Cox, T.J. Skousen, J.A. Ohlhausen, M.W. Jenkins, B. Jokiel, T.B. Parson, S.A. Candelaria, M.A. Duesterhaus and S.J. Timpe, "Acceleration of Dormant Storage Effects to Address the Reliability of Silicon Surface Micromachined Micro-Electro-Mechanical Systems (MEMS)," **SAND2008-036903693362** (2006) Sandia National Laboratories, Albuquerque, New Mexico.

1.4 M.J. Stevens, "Thoughts on the Structure of Alkylsilane Monolayers," *Langmuir* **15** (1999) p.2773-2778.

1.5 M.T. Dugger, R.J. Hohlfelder and D.E. Peebles, "Degradation of Monolayer Lubricants for MEMS," *Proc. SPIE - The International Society for Optical Engineering,* **4980** (2003) p.138-150.

1.6 D.A. Hook, S.J. Timpe, M.T. Dugger and J. Krim, "Tribological Degradation of Fluorocarbon Coated Silicon MEMS in Normal and Sliding Contact," submitted to *J. Applied Physics*.
1.7 T.W. Scharf, S.V. Prasad, M.T. Dugger, P.G. Kotula, R.S. Goeke and R.K. Grubbs,"Growth, Structure, and Tribological Behavior of Atomic Layer-Deposited Tungsten Disulphide Solid Lubricant Coatings with Applications to MEMS," *Acta Materialia* **54** (2006) p.4731-4743.
1.8 W.R. Ashurst, Y.J. Jang, L. Magagnin, C. Carraro, M.M. Sung and R. Maboudian, "Nanometer-thin titania films with sam-level stiction and superior wear resistance for reliable mems performance," Proceedings of the IEEE International Conference on Micro Electro Mechanical Systems (MEMS), Jan 25-29 2004; Maastricht, Netherlands, p.153-156.
1.9 D.A. LaVan and T.E. Buchheit, "Testing of Critical Features of Polysilicon MEMS," *Materials Research Society Symposium Proceedings* **605** (2000) p.19-24.
1.10 W.R. Ashurst, M.B.J. Wijesundara, C. Carraro and R. Maboudian, "Tribological Impact of SiC Encapsulation of Released Polycrystalline Silicon Microstructures," *Tribology Letters* **17** (2004) p.195-198.
1.11 K. Strawhecker, D.B. Asay, J. McKinney and S.H. Kim, "Reduction of Adhesion and Friction of Silicon Oxide Surface in the Presence of n-Propanol Vapor in the Gas Phase," *Tribology Letters* **19** (2005) p.17-21.
1.12 D.B. Asay and S.H. Kim," Molar Volume and Adsorption Isotherm Dependence of Capillary Forces in Nanoasperity Contacts," *Langmuir* **23** (2007) p.12174–12178.
1.13 D.B. Asay, M.T. Dugger, J.A. Ohlhausen and S.H. Kim, "Macro- to Nano-Scale Wear Prevention Via Molecular Adsorption," *Langmuir* (in press).
1.14 D.B. Asay, M.T. Dugger and S.H. Kim, "In-Situ Vapor Phase Lubrication of MEMS," *Tribology Letters* (in press).

2. Experimental Approach

2.1 Vapor Generation and Supply

A gas supply apparatus was developed to produce a N_2 stream containing the desired concentrations of water vapor and 1-pentanol for friction and wear testing. A schematic illustration of the apparatus is shown in Figure 2.1. This apparatus was deployed for both the MEMS test chamber and the glovebox containing a sphere-on-flat friction tester described below. The apparatus consisted of a manifold in which three gas streams were mixed. One gas stream went from the lab dry N_2 supply through a flow meter and to the manifold. Another gas stream went from the dry N_2 supply through a flow meter and then two bubblers in series, each containing filtered deionized water. The third gas stream went from the dry N_2 supply through a flow meter and then two bubblers in series

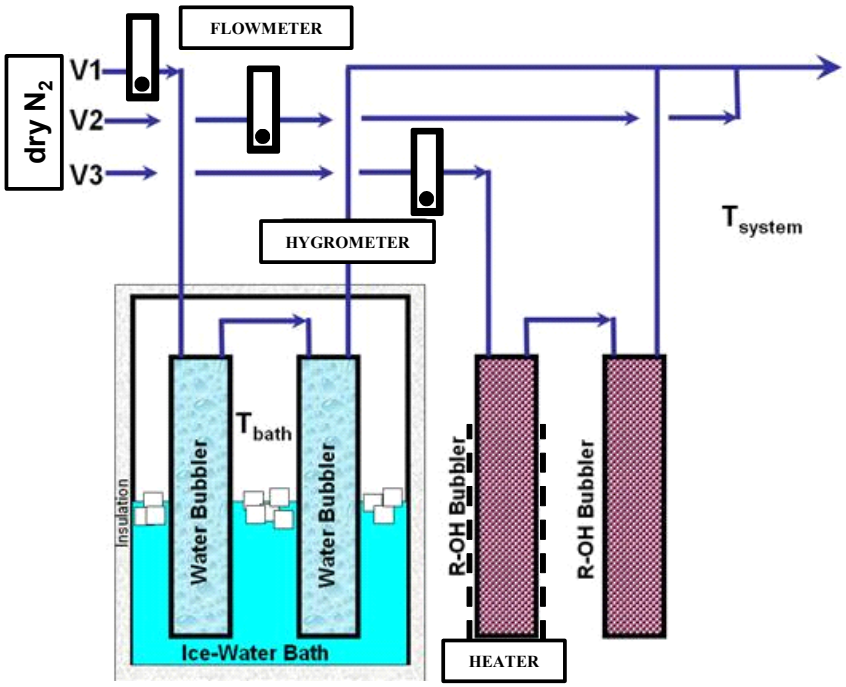

Figure 2.1 Schematic of the apparatus for generating N_2 saturated with water vapor or pentanol, and mixing with dry N_2 to achieve the desired enviroment.

containing reagent grade 1-pentanol. The bubblers consisted of 5 cm inner diameter by 20 cm tall polyethylene graduated cylinders filled with glass beads. Two polyethylene tubes 6.25 mm in outer diameter were used to deliver N_2 to and from the cylinders through a rubber stopper. One tube supplied the gas to the bottom of the cylinder through a gas diffuser. The other tube just extended into the stopper, and allowed the gas from the top of the cylinder to flow downstream. In this way, N_2 gas saturated with the desired amounts of water and 1-pentanol could be generated, mixed at the manifold, and supplied to the tester. To keep the saturated water vapor concentration in the desired range, the water bubblers were kept in an outer bath of ice water to reduce the saturation partial pressure of water. To ensure that the pentanol stream was saturated, the first bubbler was

warmed slightly with a heating pad and the other left at room temperature. In this way, gas supersaturated with pentanol at room temperature would exit the second bubbler just at saturation at the bubbler temperature. The water concentration generated using this method was verified using a chilled mirror (General Eastern Hygro M4) to measure the dew point of gas from the water bubbler alone at a flow rate of 0.5 L/min. The measured dew point agreed to within 1ºC of the temperature of the bath, when tested at both 0ºC and 21ºC. The concentration of the alcohol stream could not be measured directly due to incompatibility of the chilled mirror sensor with alcohol vapors, but was assumed to be saturated at the temperature of the second bubbler (21ºC).

It should be noted that these experiments can be very dangerous in large test volumes, for different alcohol species than the pentanol selected for this work. The test chambers are purged with nitrogen and the lack of oxygen was verified with an oxygen analyzer before introducing alcohol and water vapors. However, an oxygen leak or inadvertent introduction of oxygen by opening the chamber could produce an explosive gas mixture with some alcohols, particularly if there are ignition sources inside the test chamber. Pentanol was selected for this work because even at the saturation pressure at room temperature, the gas mixture is below the flammability limit. Care should be exercised when working with alcohol vapors, using engineering controls or fundamental physical limits as in this case to insure that there is no possibility of ignition.

2.2 Macroscale Sphere-on-Flat

Sphere-on-flat friction and wear experiments were conducted using a home-built tribometer in a controlled environment glovebox. The glovebox was purged continuously with dry N_2 at a flow rate of ~ 2 L/min. A separate 6.25 mm outer diameter polyethylene gas supply line was installed from the wall of the glovebox to a clamp that held the free end of the tube within 1 cm of the sliding interface. Since this gas mixture was delivered to the tube 1 cm from the contact region at 0.5 L/min, the test environment was assumed to be represented by the mixture of gases established by the vapor generation and supply apparatus described above.

The mechanical contact in this test consisted of a 3.125 mm diameter quartz (SiO_2) ball sliding on a Si(100) wafer at a speed of 1.5 mm/s with an applied load of 98 mN. Each test was performed with fresh surfaces. Silicon wafers with native oxide layers were cleaved to create ~1 cm square samples for testing. These samples and the quartz balls were ultrasonically cleaned in acetone and propanol, and then blown dry with N_2. The samples were further cleaned in a UV/ozone chamber (Jelight Company, model 144AX) for 15 minutes just before testing. A schematic illustration and image of the tester are shown in Figure 2.2.

2.3 MEMS Tribometer

The MEMS devices were made up of polycrystalline silicon layers 2 μm thick that were initially separated by silicon dioxide layers of similar thickness. The silicon and oxide layers were patterned to create complex structures and electrostatic actuators, using the SUMMiT V polysilicon surface micromachine fabrication process [2.1]. After etching away the oxide layers in hydrofluoric acid, the surfaces were rinsed in water, and then

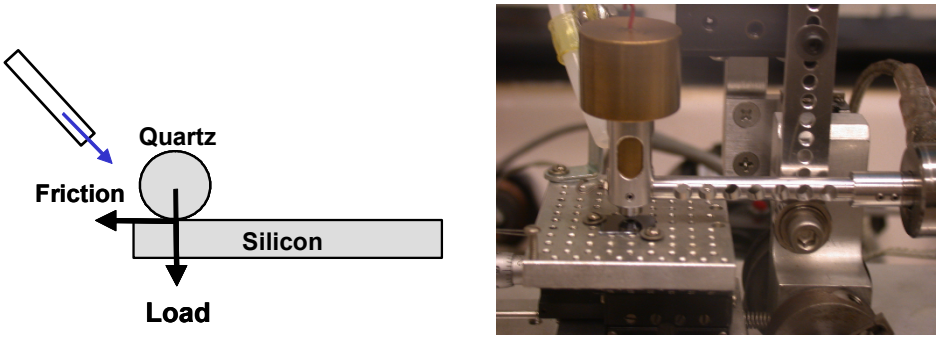

Figure 2.2 Schematic of the sphere-on-flat test apparatus (a), and an image of the test device showing the weights for loading and gas delivery tube (b).

transferred to methanol by solvent exchange while maintaining the surfaces flooded with fluid to avoid capillary attraction and collapse of the structures. The methanol was then extracted in supercritical CO_2 to avoid capillary formation. These devices were treated with a chemisorbed organic monolayer to make the surfaces hydrophobic [2.2]. The fluorinated monolayer [tridecafluorotris(dimethylamino)silane, or FOTAS, $CF_3(CF_2)_5(CH_2)_2Si(N(CH_3)_2)_3$] was applied by exposing cleaned surfaces to the molecule in a vacuum chamber at a total pressure of 2 mTorr for 12 minutes.

A diagnostic device for measuring friction in surface micromachined MEMS was used to demonstrate operation of a device in environments containing water vapor. The device is the same as that used previously [2.3], and was fabricated using the Sandia National Laboratories SUMMiT process.

The device is shown in Figure 2.3, and was operated by applying a waveform to the slide actuator that would yield constant velocity sliding for an amplitude of ~12 μm at an operating frequency of 100 Hz, yielding a sliding velocity of 1.2 mm/s. While the device

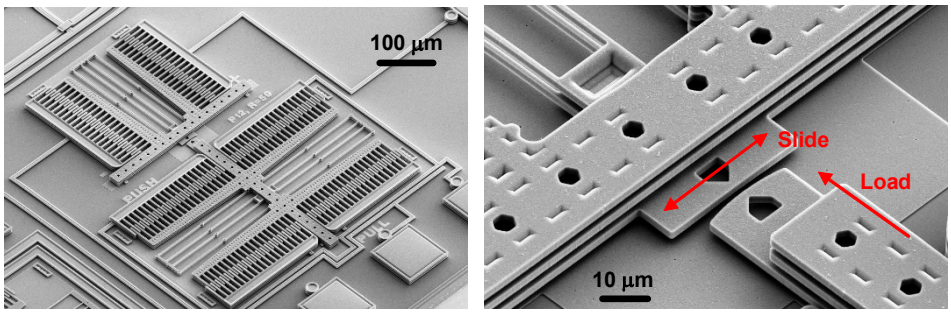

(a) (b)

Figure 2.3 SEM image of the MEMS tribometer showing the entire device with actuators (a) and a detail of the contact area (b).

was oscillating at this amplitude, A_o in the absence of contact, the normal load was ramped up to 500 nN over a period of a few seconds. The new instantaneous amplitude, A, will be less than that without contact due to the influence of friction at the contact point. The device amplitude results in a balance between the electrostatic force, the

suspension spring stiffness, and friction. Therefore, monitoring the device amplitude as a function of contact time allows the friction force to be calculated if the spring stiffness and electrostatic force are known.

Previous experiments showed that with the chemisorbed FOTAS monolayer alone, the MEMS tribometer would operate for less than 10^4 cycles in dry N_2, while in the presence of alcohol vapors no failures were observed up to 10^8 sliding cycles [2.4]. Therefore in order to explore several gas mixtures, screening tests were run for 10^6 cycles in various environments. In this way, a significant number of environments were surveyed with a simple MEMS device to verify operation in the presence of water vapor and alcohol vapor. The same vapor generation and delivery system as described for the macroscopic sphere-on-flat tests were used for the MEMS device tests, by flowing the controlled environment through the chamber shown in Figure 2.4.

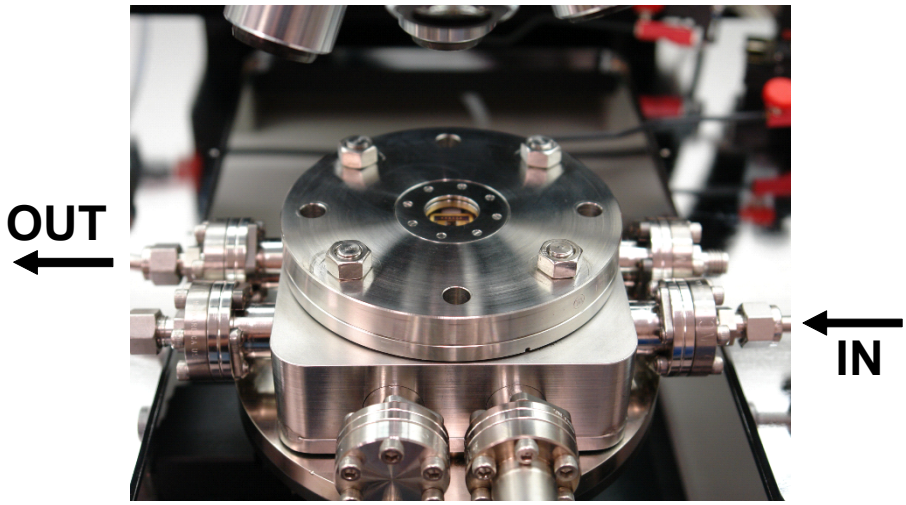

Figure 2.4 Image of the controlled environment chamber for MEMS device testing. The circular top cover is a 4.5 inch diameter conflat flange.

2.4 MEMS Gear Train

A scanning electron microscope image of the MEMS gear train device is shown in Figure 2.5. It consists of a total of six gears driven by electrostatic actuators. This device was chosen because it contains numerous locations of surface contact, including dimples, gear teeth and gear hubs, and a significant amount of characterization of the operating life of the device has previously been done. This device is part of a prototype weapon surety system known as the "discriminating microswitch," or DMS.

The voltage waveforms to operate the device were identical to those previously used to characterize the operating life of the device and are shown in Figure 2.6. The drive signals are essentially 90 V square waves, applied to the left, up, right, and down actuators in sequence to drive the output gear around on its hub. These waveforms were

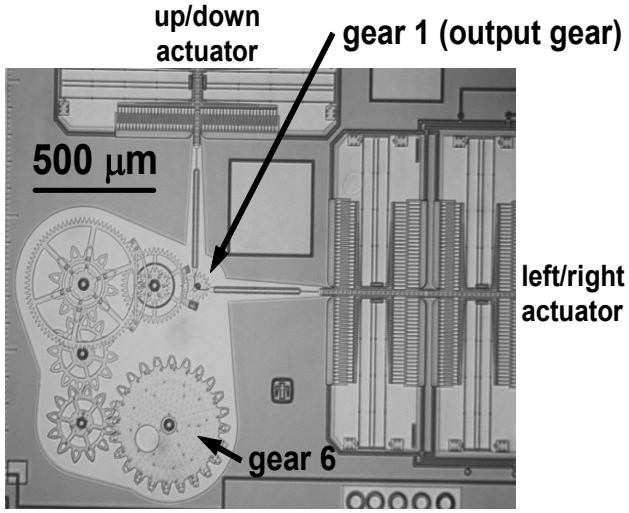

(a)

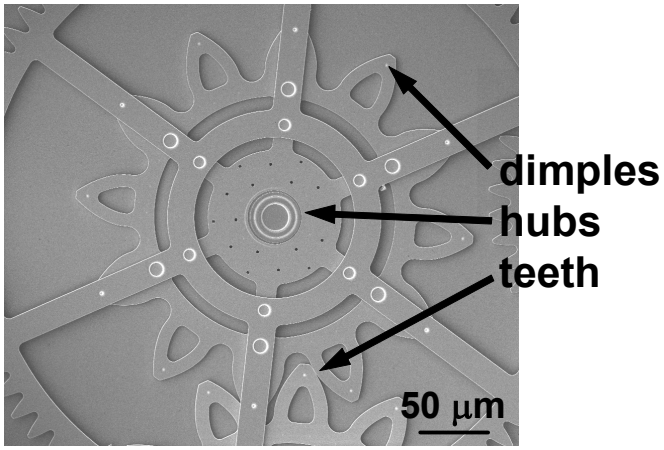

(b)

Figure 2.5 SEM image of the MEMS test device showing gears and electrostatic actuators (a), and a detail of gear 3 with contact locations (b).

originally selected because they are relatively simple for weapon on-board circuitry to generate. However, these waveforms result in significant radial forces. The waveforms shown will cause the output gear to make one revolution. The large gear (gear 6) is designed to rotate 270 degrees from reset to enable, and then 270 degrees in the opposite direction back to its starting point. Due to the gear ratio, this motion requires that the small output gear be rotated 16 revolutions in one direction, and then reversed and rotated 16 revolutions in the opposite direction. Waveforms were designed for the arbitrary waveform generators so that one period contained 32 of the wave periods shown in Figure 2.6, for the 16 forward and 16 reverse output gear rotations corresponding to +/- 270 degree rotation of the final gear. Operating life was defined as the number of revolutions of the small output gear until it failed to make a full revolution using the applied drive signals. The device was operated in the same environmental chamber as the MEMS tribometer.

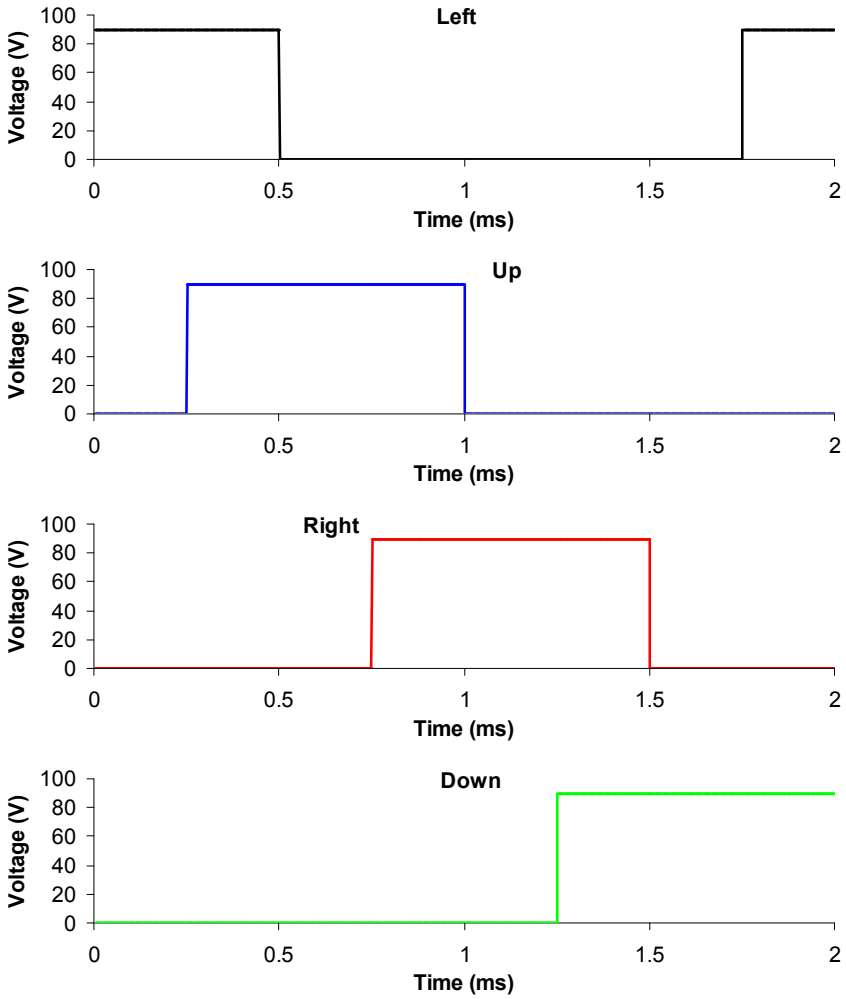

Figure 2.6 Waveforms applied to the left, up, right, and down actuators of the MEMS gear train to cause the output gear to rotate at 500 Hz.

2.5 ToF-SIMS Surface Analysis

Time-of-flight secondary ion mass spectrometry (ToF-SIMS) spectral imaging was performed (Physical Electronics TRIFT I) using a pulsed and bunched 15 kV, 600 pA $^{69}Ga^{+}$ beam rastered over a 140 μm x 140 μm area for five minutes while acquiring positive secondary ions. Bunched mode was used for high mass resolution to aid in peak identification. For high-resolution imaging, a pulsed 25 kV, 600 pA $^{69}Ga+$ beam was used. A five minute acquisition in a 140 μm x 140 μm region was also employed in this mode. Multivariate analysis was performed using AXSIA (Automated eXpert Spectral Image Analysis) developed at Sandia National Laboratories [2.5]. The multivariate curve resolution method was used to separate the spectral image into its unique components.

2.6 Microscopy and Wear

Imaging of worn devices, as well as sectioning to examine interior structures, was performed using a dual beam focused ion beam (FEI DB 235) system. This instrument enabled both high resolution imaging of contact surfaces to search for wear debris, and

sectioning through gear hubs to search for reaction product accumulated at deeply buried sliding surfaces.

Wear tracks from the sphere-on-flat experiments were examined using white light interferometry (Wyko NT1100D). The topography of the wear scar was measured, and the wear volume computed as the amount of material displaced from the original unworn surface. Three measurements were taken on each wear scar.

Chapter 2 References

2.1 M.S. Rogers and J.J. Sniegowski, "5-Level Polysilicon Surface Micromachine Technology: Application To Complex Mechanical Systems," *Technical Digest, Solid-State Sensors and Actuators Workshop,* Hilton Head Island, SC, 1998; p.144-149.

2.2 M. G. Hankins, P. J. Resnick, P. J. Clews, T. M. Mayer, D. M. Tanner, and R. A. Plass, "Vapor Deposition of Amino-Functionalized Self-Assembled Monolayers on MEMS," in *Proc. SPIE - The International Society for Optical Engineering,* **4980** (2003) R. Ramesham and D.M. Tanner, Eds., p.238–247.

2.3 D.B. Asay, M.T. Dugger, J.A. Ohlhausen and S.H. Kim, "Macro- to Nano-Scale Wear Prevention Via Molecular Adsorption," *Langmuir* (in press).

2.4 D.B. Asay, M.T. Dugger and S.H. Kim, "In-Situ Vapor Phase Lubrication of MEMS," *Tribology Letters* (in press).

2.5 V.S. Smentkowski, J.A. Ohlhausen, P.G. Kotula and M.R. Keenan, "Multivariate Statistical Analysis Of Time-Of-Flight Secondary Ion Mass Spectrometry Images - Looking Beyond The Obvious," *Applied Surface Science* **231** (2004) p.245-249.

3. Results and Discussion

3.1 Effects of Water Vapor on VPL by Pentanol

The results of sphere-on-flat friction tests in mixed alcohol and water vapor environments are shown in Figure 3.1. A worst case baseline of 1000 ppmv water vapor was chosen for the mixed environments since previous analyses of MEMS packages [3.1] have shown that this level of water vapor can be easily attained within ceramic DIP packages using conventional packaging technology, without a getter for water.

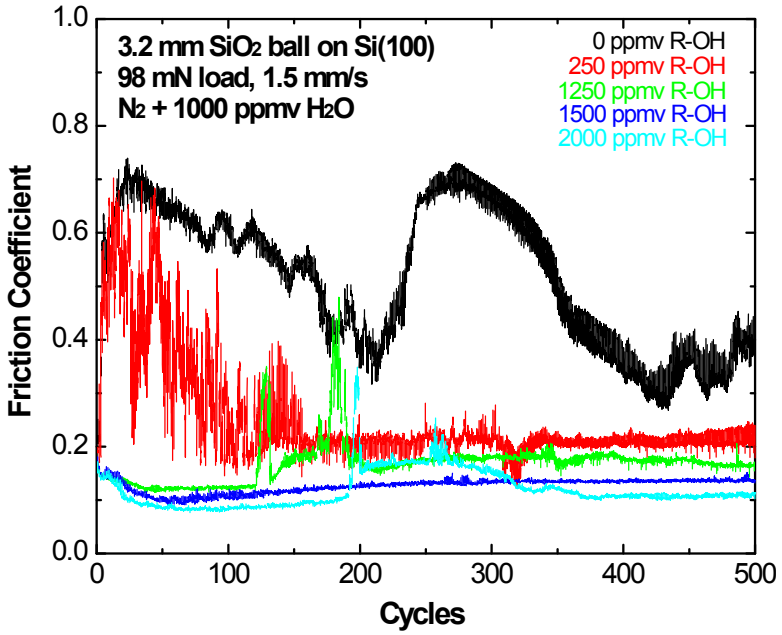

Figure 3.1 Friction coefficient versus cycles for sphere-on-flat tests in N_2 with 1000 ppmv water vapor containing various concentrations of pentanol vapor.

The figure shows that with no alcohol vapor present, the friction coefficient rapidly increases to ~0.7. Throughout sliding, the friction coefficient fluctuates dramatically due to generation of wear debris, and then the debris getting pushed out of the contact. The interface changes between two body and three body sliding depending on the presence of debris in the contact.

This experiment was repeated with alcohol vapor added to the gas stream flowing to the contact region, in increments of 250 ppmv pentanol. Each trace represents a new test with fresh surfaces. Figure 3.1 shows that while the first 250 ppmv pentanol addition to the test environment has an influence on friction coefficient evolution, the early stage friction remains high and erratic up to a pentanol concentration of about 1500 ppmv. For this and higher alcohol concentrations, the friction coefficient rarely exceeds 0.2.

Wear measurements from the above macroscale sliding experiments are given in Figure 3.2, which shows the wear volume as a function of pentanol concentration. Similar to the friction measurements, a dramatic decrease in wear was observed as pentanol vapor was

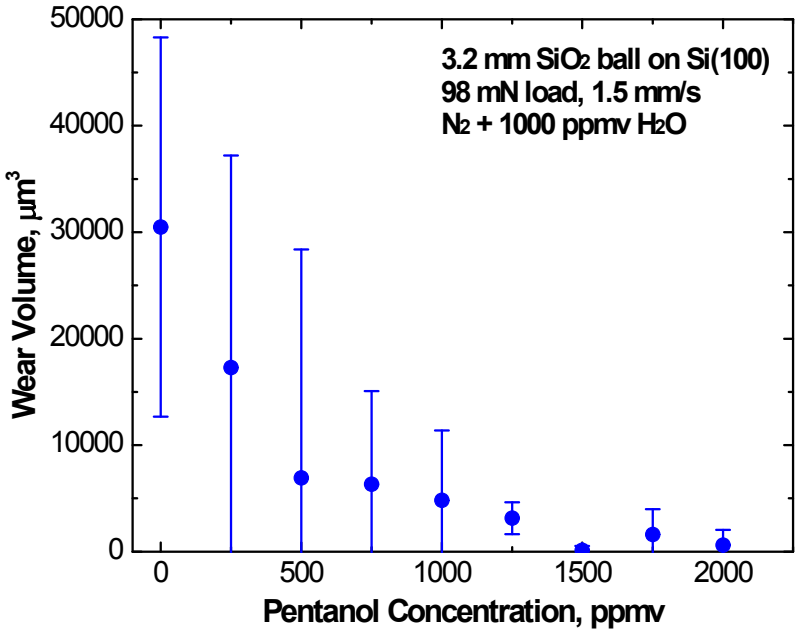

Figure 3.2 Wear volume from the sphere-on-flat experiments as a function of pentanol vapor concentration in N_2 with 1000 ppmv H_2O.

added to the sliding environment. The wear volume at 1500 ppmv pentanol and above was near the resolution limit of the instrument.

The friction and wear data indicate that the presence of water vapor does not inhibit the vapor phase lubrication of silicon by pentanol. However, a higher concentration of pentanol is required to achieve low friction and low wear when water vapor is present. The highest concentration of pentanol used in these experiments (2000 ppmv) is close to the maximum achievable at a room temperature of 21°C, given the saturation pressure of pentanol of 2.031 mbar at this temperature [3.2].

ToF-SIMS analysis was performed on the wear track from the test at 2000 ppmv pentanol. Figure 3.3 shows the component at the center of the wear track (panel a) along with its ion spectrum (panel c), compared to a wear track from a test in N_2 with pentanol alone (panel b). The AXIA analysis shows that the same compound is being formed in the tests containing water vapor and pentanol as is formed with pentanol alone, although the amount of reaction product formed is greater in the absence of water vapor.

Based on these experiments, it appears that VPL with alcohol can be achieved when the alcohol to water vapor concentration is at least about 2:1. This may be challenging for water vapor concentrations as high as 1000 ppmv, but the water vapor can be reduced by including a getter in the package. Additionally, an alcohol with higher vapor pressure can be used to generate larger alcohol vapor concentrations at the test temperature. Therefore, it appears that even with realistic levels of water vapor present, vapor phase lubrication is a viable approach for packaged MEMS.

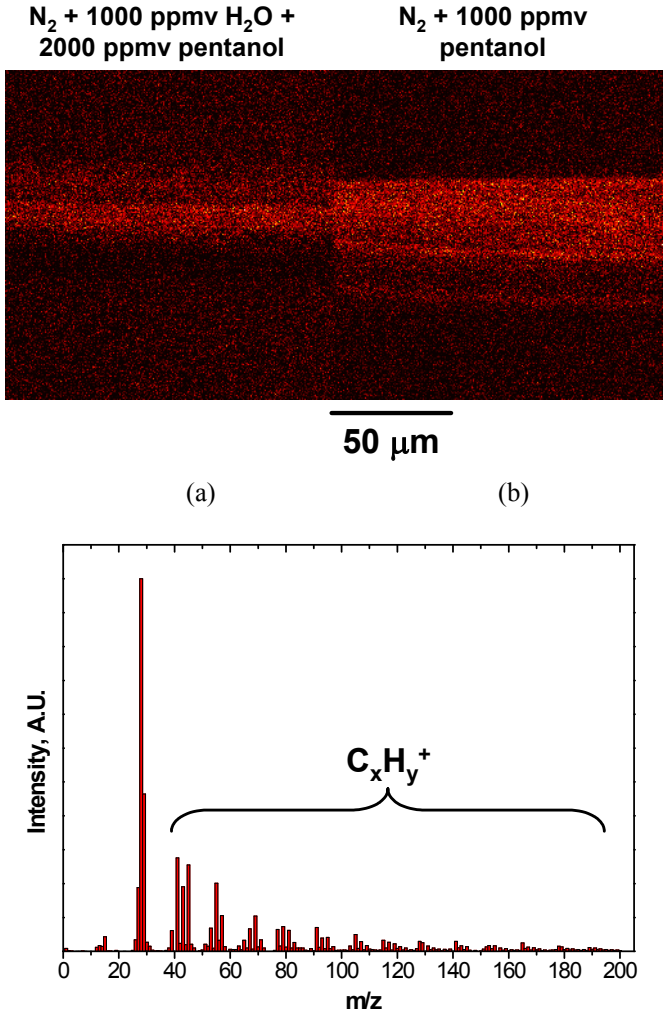

Figure 3.3 Spatial location of high molecular weight component in wear tracks from tests with (a) and without (b) water vapor, and the associated positive ion spectrum from AXIA (c).

3.2 MEMS Tribometer Operation

The results of select tests with the MEMS tribometer in mixed water vapor and alcohol environments are shown in Table 3.1. The table shows water concentrations from 0 to 1000 ppmv in columns, and pentanol concentrations from 0 to 2000 ppmv in rows. The colored blocks indicate a mixture of water vapor and pentanol vapor where an experiment was performed. The resulting cycles to failure (or when the device was stopped) are listed as entries in the table. For example, the table indicates that with no water vapor present, the device failed within 5,000 cycles in dry N_2, but operated for 10^6 cycles for pentanol concentrations of at least 500 ppmv. The table also shows that at 1000 ppmv water vapor and no pentanol, the device also failed very quickly, at 4,000 cycles. At 500

Table 3.1 Operating Life of MEMS Tribometer in Mixed Pentanol and Water Vapor Environments

1-Pentanol ppmv \ WATER ppmv	0	250	500	750	1000
0	$5x10^3$				$4x10^3$
500	$1x10^6$				
1000			$1x10^6$		
1500					
2000	$1x10^6$		$1x10^6$		$5x10^5$

ppmv water vapor, the devices tested with 1000 and 2000 ppmv pentanol vapor both completed the screening test and ran the full 10^6 cycles without failure, and were stopped. The test at 1000 ppmv water and 2000 ppmv pentanol ran much longer than in environments without pentanol, but failed at $5x10^5$ cycles.

Examples of the displacement amplitude history of the MEMS tribometer operating in the environments shown in Table 3.1 are shown in Figure 3.4. The tests in dry nitrogen failed almost immediately on this scale, as shown at the lower left corner of the plot. The amplitude history of the test at 500 ppmv water and 2000 ppmv pentanol shows consistent behavior throughout the test. However, the test at 1000 ppmv water vapor and 2000 ppmv pentanol shows more variation throughout the test, until failure at $5x10^5$ cycles where the displacement amplitude goes to zero.

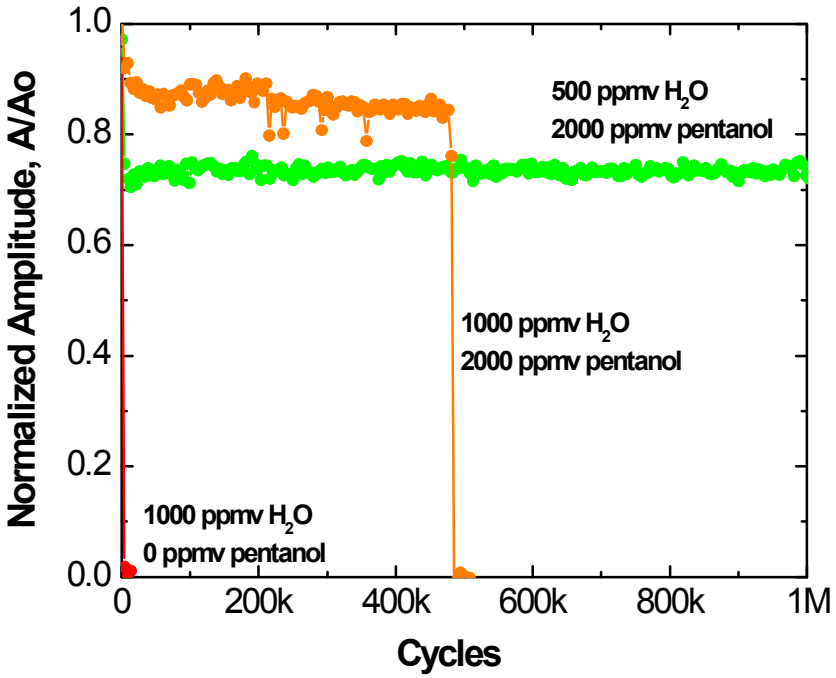

Figure 3.4 Oscillation amplitude of MEMS tribometers as a function of cycles operating in various environments, normalized to the out of contact amplitude A_o.

An SEM image of the worn surface from the MEMS tribometer that failed at $5x10^5$ cycles is shown in Figure 3.5. There is no detectable damage to the sliding surface, as was observed in tests without water vapor (not shown). However, the top planar surface of the polycrystalline silicon contains a few particles (indicated by arrows) which may be the result of wear processes that created particles that were then pushed out of the contact and collected adjacent to the sliding surface.

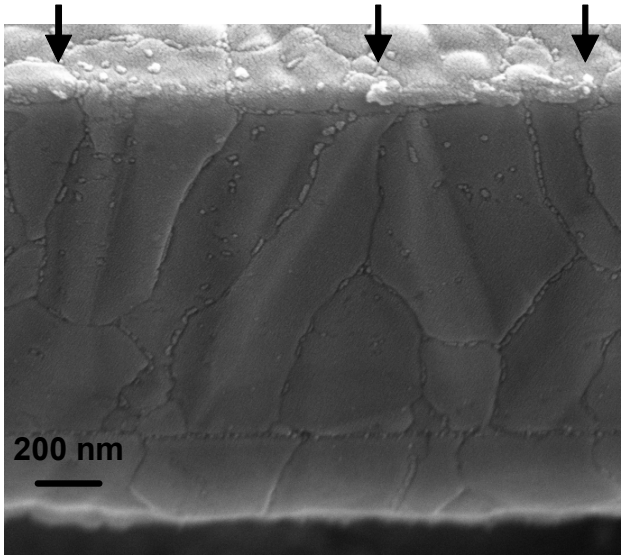

Figure 3.5 SEM image of the sidewall surface of the MEMS tribometer that was in contact with a similar mating surface in N_2 with 1000 ppmv water vapor and 2000 ppmv pentanol. This device ceased operation at $5x10^5$ cycles. Arrows mark the locations of possible debris particles.

3.3 Lubrication of the MEMS Gear Train

The MEMS gear train was previously operated in MEMS reliability studies [3.3], and the failure distribution that was determined is shown in Figure 3.6. This figure indicates that when operated in air, which gave the longest operating life, the median cycles to failure were 4.7×10^4 at 500 Hz. When operated in a N_2 environment with 1000 ppmv pentanol, this device operated for 4.8×10^8 cycles without failure, until the test was stopped. Although the device did not fail, it was stopped after running for more than 11 days so that the test equipment could be used for other experiments.

In an attempt to cause failure of the device, higher operational frequencies were explored to accumulate cycles on the gear more quickly. It was found that the device would operate with the same drive signals as discussed above, but at 4.17 kHz. The resulting speed of the output gear (gear 1) was 250,000 rev/min compared to 30,000 rev/min in the test described above. The device would not operate reliably at higher frequency than this due to inertial loads of all the gears in the series. Another test was run with a fresh device at 1000 ppmv pentanol using the higher operating frequency. The device failed to make a complete revolution of the small gear after $7.12x10^8$ cycles. Electron microscopy

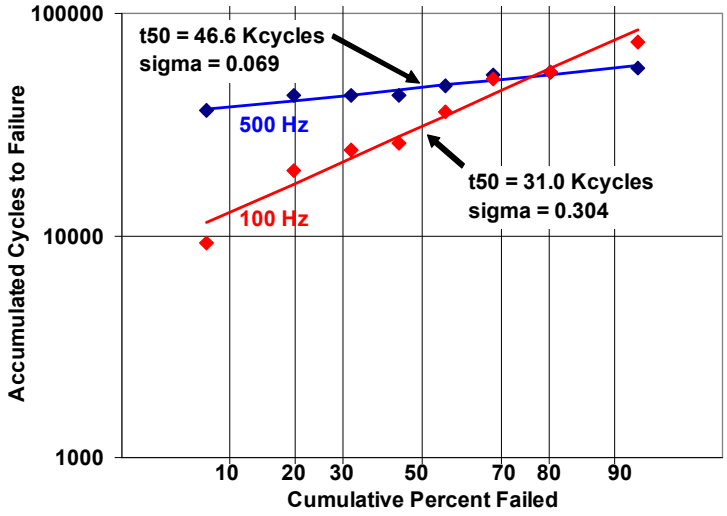

Figure 3.6 Failure distributions of the MEMS gear train operated in air with FOTAS monolayer alone, at 100 Hz and 500 Hz output gear 1 frequency [3.3].

was used to search for evidence of wear on this gear train. Figure 3.7 shows the result of examination of select contact areas for wear. A few debris particles were observed at the hub of gear 1 (panel a). All of these devices were subjected to less than 100 revolutions of the small gear in air to verify functionality. The amount of debris seen on the device tested with pentanol vapor is similar to that seen on devices after the functional tests alone (panel b). Therefore, the debris seen in the high frequency test is believed to have been present before the alcohol VPL experiment was conducted, and the result of functional testing. A FIB section was taken through the hub of gear 1, and no significant wear could be seen at the hub or pin joint (panel c). Closer inspection of the interface between the pin joint and the gear (panel d) did reveal some material that appears to bridge the moving surfaces. This deposit was not observed in devices operated without alcohol vapors, and is believed to be the reaction product between the silicon surfaces and the adsorbed alcohol. Unfortunately, this deposit is too small to test with ToF-SIMS, and the orientation of the vertical section is not conducive for analysis.

Finally, in an effort to determine whether the high molecular weight reaction product had formed in the high frequency test, gear 3 was removed by making a circular FIB cut around the hub. The entire gear could then be lifted off the device and flipped over so that the underside of the gear and the substrate beneath the gear could be analyzed. Figure 3.8 shows a dimple on the bottom of gear 3, with no evidence of wear or particle accumulation. The substrate reveals a circular arc where it was covered by the tooth, corresponding to the path of the dimple around the hub as the gear rotates. The full circular path of the dimples could not be seen since this device was sputter coated with a thin layer of AuPd to mitigate charge build up and improve imaging. Chemical identification of the dark track in Figure 3.8b was attempted with ToF-SIMS, but the component could not be conclusively identified due to the AuPd creating extra components in the AXIA analysis, and the small size of the track.

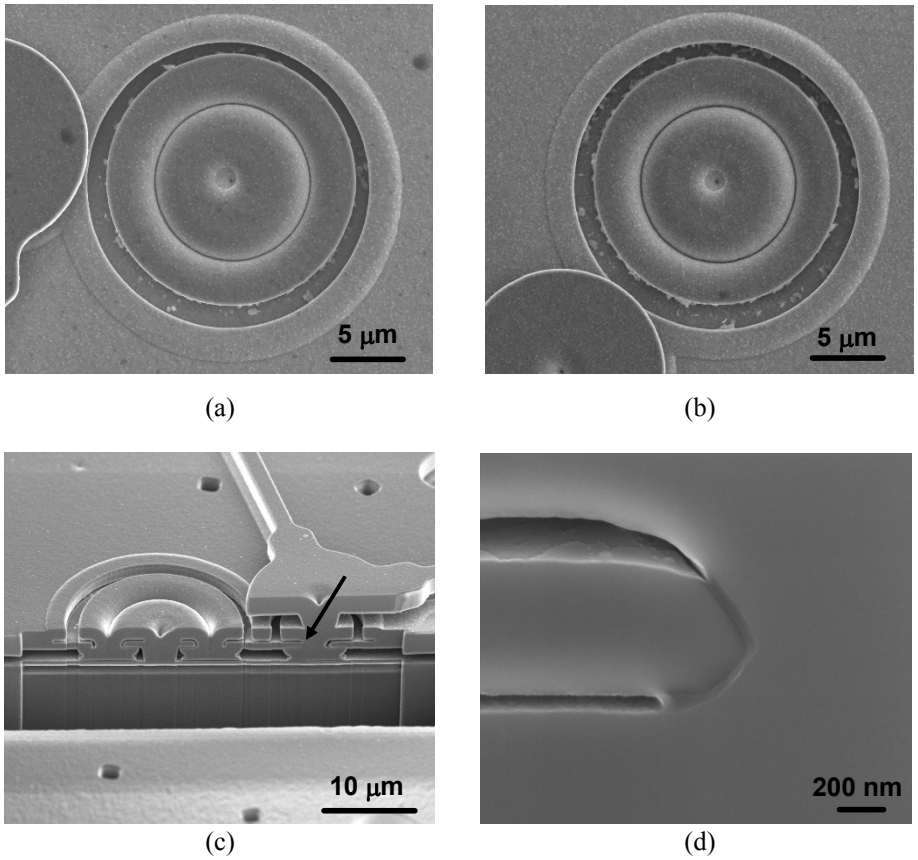

Figure 3.7 The hub of gear 1 from a MEMS gear train operated to 7.12×10^8 cycles in pentanol vapor (a), and another device operated for 100 cycles in air (b). A FIB section through the hub in (a) is shown in panel (c), with the arrow marking the pin joint-gear interface detailed in panel (d).

In summary, tests of alcohol vapor phase lubrication of a complex MEMS device with numerous contacts were successful. The device operated at least four orders of magnitude longer with VPL than it did with the FOTAS monolayer alone, using identical actuation waveforms and frequency conditions. The only failure that was produced occurred when the device was operated as fast as possible given the inertial loads of the gears, and this device operated for 7.12×10^8 cycles. Even after the device failed to make a full revolution using these drive signals, the device was not "stuck," and the gears would continue to oscillate partially around the hub. In fact, when the drive frequency was reduced to 500 Hz, the device would once again make full revolutions and continue to operate. The failure at high frequency, with continued operation at low frequency, is consistent with the presence of a reaction product at the deeply buried contacts in the device that adds viscous damping during motion. The FIB sections and images suggest the presence of a reaction product at sliding interfaces, although its chemical composition could not be determined.

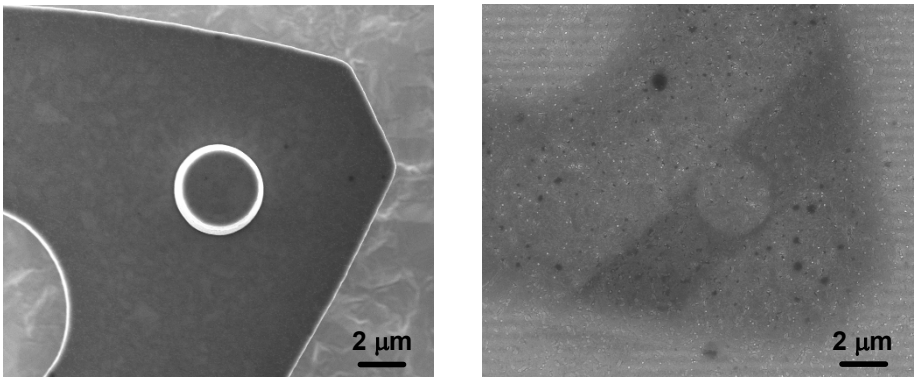

(a) (b)

Figure 3.8 The bottom surface of a tooth on gear 3, after it was FIB cut from the device and flipped over to examine the dimple (a). The substrate under a tooth of gear 3 is shown in (b).

Chapter 3 References

3.1. S.M. Thornberg, J.R. Brown, M.S. Kent, K.R. Zavadil, T.A. Ordonez, J.A. Ohlhausen, D.R. Tallant, M.J. Garcia and R.L. Simpson, "MEMS Characterization LDRD: Final Report (FY03-FY05)," SAND2008-036903697083, Sandia National Laboratories, Albuquerque, New Mexico, 2005.

3.2 The vapor pressure versus temperature for pentanol was calculated using the Antoine equation parameters given in: D. Ambrose, C.H.S. Sprake and R. Townsend, "Thermodynamic Properties of Organic Oxygen Compounds. XXXVII. Vapour Pressures of Methanol, Ethanol, Pentan-1-ol, and Octan-1-ol from the Normal Boiling Temperature to the Critical Temperature," *J. Chem. Thermodyn.* **7** (1975) p.185-190.

3.3 Data on the MEMS gear train operated in air is courtesy of Danelle Tanner, org. 1749-1, unpublished.

4. Conclusions and Recommendations

4.1 Conclusions

Vapor phase lubrication of silicon surfaces using pentanol was found to produce extraordinary increases in the operating life of MEMS devices. Macroscale sphere-on-flat testing suggests that this increase is due to the formation of a high molecular weight reaction product at real contact locations that prevents wear and maintains friction coefficient near 0.2 by passivating active sites on the surface. Water vapor does appear to interfere with reaction product formation, but VPL with pentanol was still effective if the alcohol to water vapor ratio can be maintained at 2:1 or higher. Effective MEMS lubrication in mixed alcohol and water vapor environments was confirmed in both macroscale tests and with MEMS tribometers.

A complex MEMS gear train was effectively lubricated with pentanol vapors, and resulted in a factor of at least 10^4 increase in operating life without failure. Failure could be induced by operating the device at much higher frequencies than previously used, and there is some evidence that the failure was due to increased damping caused by reaction product formation at deeply buried sliding interfaces. If heated asperity contacts, or emission of low energy electrons from heated asperity tips are important in the reaction product formation, reaction product formation would be exacerbated by high interfacial velocities and this type of failure may not be relevant to real applications.

The mechanisms considered as potential show stoppers for application of VPL to packaged MEMS devices do not appear to be significant barriers to implementation.

4.2 Recommendations

Successful lubrication of silicon surfaces has been demonstrated with alcohol vapors, from the MEMS scale to the macroscale. However, the fundamental reaction pathways responsible for the observed improvements in performance are not understood. The Lewis acid character of the substrate, thermal decomposition of alcohols at heated asperity contacts, or thermionic emission of low energy electrons are among the possible mechanisms responsible for reaction product formation. A fundamental examination of reaction mechanisms in vapor phase lubrication is recommended so that precursor chemistry may be selected to optimize film properties, and so that this approach may be applied to other surfaces. In addition, the kinetics of reaction product formation should be examined. An understanding of reaction kinetics is required to define the range of interfacial velocities for which successful lubrication can be expected as a function of partial pressure of the alcohol, substrate temperature, and substrate composition.

A limited number of macroscale sphere-on-flat tests using other materials suggests that VPL with pentanol is very effective on stainless steel as well. Therefore the potential benefits of this approach may extend well beyond applications to silicon MEMS. Vapor phase lubrication may offer an alternative lubrication approach for conventionally fabricated metal alloy parts for weapons systems.

Distribution:

1	MS0886	J.A. Ohlhausen	1822
1	MS0889	J.S. Custer	1824
1	MS0889	M.T. Dugger	1824
1	MS0889	S.V. Prasad	1824
1	MS1064	M.A. Polosky	2614
1	MS1064	E.J. Garica	2614
1	MS1069	M.S. Baker	1749-2
1	MS1069	D.A. Czaplewski	1749-2
1	MS1069	T.B. Parson	1749-1
1	MS1069	M.R. Platzbecker	1749-1
1	MS1069	D.M. Tanner	1749-1
1	MS1080	D. Luck	1749-1
1	MS1080	K. Ortiz	1749
1	MS1080	M.J. Shaw	1749-1
1	MS1084	P.J. Clews	1746
1	MS9018	Central Technical Files	8944
1	MS0899	Technical Library	9536 (electronic copy)
1	MS0123	D.L. Chavez, LDRD Office	1030